MIL-50, an Open-Framework GaPO with a Periodic Pattern of Small Water Ponds and Dry Rubidium Atoms: a Combined XRD, NMR, and Computational Study

Lionel Beitone,[†] Jérôme Marrot,[†] Thierry Loiseau,*,[†] Gérard Férey,[†] Marc Henry,[‡] Clarisse Huguenard,[‡] Axel Gansmuller,[‡] and Francis Taulelle[‡]

Contribution from the Institut Lavoisier, UMR CNRS 8637, Université de Versailles St Quentin en Yvelines, 45, Avenue des Etats-Unis, 78035 Versailles Cedex, France and NMR & Solid State Chemistry, Molecular Tectonics of Solid State, FRE CNRS 2423, Université Louis Pasteur, Institut Le Bel, 4, rue Blaise Pascal, 67070 Strasbourg Cedex, France

Received October 24, 2002 ; E-mail: loiseau@chimie.uvsq.fr

Abstract: A new fluorinated gallium phosphate, MIL-50, has been synthesized under mild hydrothermal conditions using 1,6-diaminohexane. The chemical formula of MIL-50 is $Rb_2Ga_9(PO_4)_8(HPO_4)(OH)F_6 \cdot 2N_2C_6H_{18} \cdot 7H_2O$. The structure is a network of hexameric units of $Ga_3(PO_4)_3F_2$ and $Ga_3(PO_4)_2(HPO_4)F_3$ via corner sharing. It creates a three-dimensional open-framework delimiting 6- and 18-ring channels running along the c axis. The diprotonated 1,6-diaminohexane and water molecules are trapped within the 18-ring pores, whereas the rubidium cations reside in the 6-ring ones. A double quantum ^{31}P NMR experiment and partial charge calculations indicate that water molecules are present under the form of periodic small clusters, lowering the multiplicity of one phosphorus site, P3. Though water hops within the clusters, the motion leaves the water pattern periodic. Rubidium is so tightly embedded into the framework that water moving in the large 18-ring channels does not reach it, leaving it therefore dry. The crystal framework may be ascribed to the orthorhombic space group $Cmc2_1$ ($n°$ 36), $a = 32.1510(2)$, $b = 17.2290(3)$, $c = 10.2120(1)$ Å. The periodic water pattern has a different symmetry than that of the framework. A method has been devised to superpose the two sublattices that coexist in the same unit cell in order to have full occupancy of each site and to perform Madelung summations. This original method is of general interest for most zeolitic materials exhibiting a different symmetry for the framework and the template sublattices.

Introduction

Since 1982, after Flanigen's first alumino-phosphate synthesis,[1] nanoporous crystalline metalophosphates have been extensively studied. These materials have many potential applications in catalysis, molecular sieves, gas separation, and ionic exchangers. They are typically prepared under mild hydrothermal conditions by using organic molecules (amines, tetralkyl-ammoniums, etc.) as structure-directing agents. The synthesis route initiated by Flanigen and co-workers[1] was furthered for designing zeolite-like three-dimensional architectures of phosphates incorporating many elements of the periodic table.[2] Gallium substitution of aluminum has retained attention since the mid 1980s, with some compounds being isotypic with their corresponding aluminophosphates.[3] Addition of fluorides, in the reaction medium, was a subsequent breakthrough, improving the mineralization process.[4] Fluorinated gallium phosphate

networks were therefore obtained. The first striking example was illustrated by the discovery of the structure of cloverite,[5] a fluorinated gallophosphate exhibiting a three-dimensional system of 20-ring channels. During the past decade, many efforts have been spent synthesizing fluorinated gallium phosphates and new compounds have been reported.[6-16] Some of these crystals adopt three-dimensional frameworks with extra-large pores. ULM-5[17] and ULM-16[18] exhibit tunnels delimited by 16 polyhedra,

---

[†] Université de Versailles St Quentin en Yvelines.

[‡] Université Louis Pasteur.

(1) Wilson, S. T.; Lok, B. M.; Messina, C. A.; Cannan, T. R.; Flanigen, E. M. *J. Am. Chem. Soc.* **1982**, *104*, 1146.
(2) Cheetham, A. K.; Férey, G.; Loiseau, T. *Angew. Chem., Int. Ed.* **1999**, *38*, 3268.
(3) Parise, J. B. *Chem. Commun.* **1985**, 606.
(4) Guth, J. L.; Kessler, H.; Wey, R. *Stud. Surf. Sci. Catal.* **1986**, *28*, 121.

(5) Estermann, M.; McCusker, L. B.; Baerlocher, C.; Merrouche, A.; Kessler, H. *Nature* **1991**, *352*, 320.
(6) Férey, G. *J. Fluorine Chem.* **1995**, *72*, 187. Férey, G. *C. R. Acad. Sci., Ser IIc* **1998**, *1*, 1.
(7) Weigel, S. J.; Weston, S. C.; Cheetham, A. K.; Stucky, G. D. *Chem. Mater.* **1997**, *9*, 1293.
(8) Wragg, D. S.; Hix, G. B.; Morris, R. E. *J. Am. Chem. Soc.* **1998**, *120*, 6822.
(9) Weigel, S. J.; Morris, R. E.; Stucky, G. D.; Cheetham, A. K. *J. Mater. Chem.* **1998**, *8*, 1607.
(10) Reinert, P.; Patarin, J.; Marler, B. *Chem. Commun.* **1998**, 1769.
(11) Reinert, P.; Patarin, J.; Marler, B. *Eur. J. Solid State Inorg. Chem.* **1998**, *35*, 389.
(12) Reinert, P.; Patarin, J.; Loiseau, T.; Férey, G.; Kessler, H. *Mic. Mes. Mat.* **1998**, *22*, 43.
(13) Wragg, D. S.; Bull, I.; Hix, G. B.; Morris, R. E. *Chem. Commun.* **1999**, 2037.
(14) Matijasic, A.; Paillaud, J.-L.; Patarin, J. *J. Mater. Chem.* **2000**, *10*, 1345.
(15) Bonhomme, F.; Thoma, S. G.; Rodriguez, M. A.; Nenoff, T. M. *Chem. Mater.* **2001**, *13*, 2112.
(16) Bonhomme, F.; Thoma, S. G.; Rodriguez, M. A.; Nenoff, T. M. *Mic. Mes. Mat.* **2001**, *47*, 185.

whereas MIL-31[19] and MIL-46[20] contain tunnels bounded by 18 polyhedra.

The formation of gallium phosphate open frameworks, with mixtures of organic template and alkaline metals, has been pursued recently in our group. The goal is the design of microporous networks inserting alkaline cations, which are well-known to be efficient for gas separation. We started a systematic study with the use of lithium. Its presence led to relatively dense solids[21,22] with no inclusion of the organic cations. Attempts were also made with rubidium. Rubidium in GaPOs was already described by Lii in $Rb_2[Ga_4(HPO_4)(PO_4)]$ 0.5 H_2O.[23] More recently, Zubieta et al. reported a vanado-gallo-phosphate $M[VO(H_2O)Ga(PO_4)_2]$ (M = Rb, Cs)[24] incorporating rubidium or cesium in the mineral network. Both compounds have a three-dimensional structure, with alkali atoms within 6-ring channels and no organic template included.

A new fluorinated gallium fluorophosphate, MIL-50, with $Rb_2Ga_9(PO_4)_8(HPO_4)(OH)F_6·2N_2C_6H_{18}·7H_2O$ as the chemical formula, has been synthesized from a mixture of 1,6-diamino-hexane and rubidium. Both reactants are present in the crystal, which exhibits an open framework, with one-dimensional 18-ring channels. XRD and NMR allowed us to determine its crystallographic structure. Additionally, a fluctuating dipolar coupling between phosphorus and hydrogen atoms occurs where some small water clusters happen to be localized, with fractional site occupancy factors. These "small water ponds" form a periodic sublattice, lowering locally the symmetry of the crystal. No water however interacts at all with rubidium atoms of the structure, leaving them "dry", a very unusual feature.

Experimental Section

Synthesis. The synthesis was carried out under mild hydrothermal conditions using gallium oxide (Ga_2O_3, Aldrich 99.99+%), phosphoric acid (H_3PO_4, Prolabo 85%), hydrofluoric acid (HF, Prolabo 48%), rubidium hydroxide (RbOH, Aldrich 50 wt % sol in water), 1,6-diaminohexane ($H_2N(CH_2)_6NH_2$, Aldrich 99%, noted DAH), and deionized water. The reactions were performed in 23 mL Teflon-lined stainless steel Parr bombs under autogenous pressure for 3 days. The molar compositions of the starting gels were 1 Ga_2O_3 (0.65 g)/2 H_3PO_4 (0.80 g)/2 HF (0.29 g)/0.5 RbOH (0.36 g)/0.6 DAH (0.25 g)/80 H_2O (4.55 g). After the resulting white product was filtered off and washed with deionized water, it was first characterized by powder X-ray diffraction (Bruker D5000, copper radiation). The results of elemental analysis for MIL-50 are Ga, 29.4%; P, 13.4%; N, 2.4%; C, 6.0%; and F, 5.3%, consistent with the calculated values deduced from the structure $Rb_2Ga_9(PO_4)_8(HPO_4)(OH)F_6·2N_2C_6H_{18}·7H_2O$: Ga, 29.2%; P, 13.0%; N, 2.6%; C, 6.7%; F, 5.3%.

Thermogravimetry. Thermogravimetry analysis was carried out on a TA instrument type 2050 thermoanalyzer under an oxygen gas flow with a heating rate of 2 °C min^{-1}. The TG curve (Figure 1) shows three events between 25 and 1050 °C. The first weight loss (6.07%) below 200 °C can be assigned to the departure of water molecules trapped within the 18-ring tunnels. This percentage corresponds to the

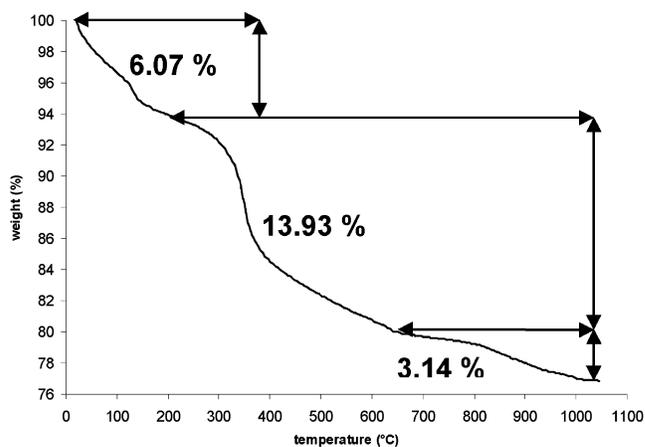**Figure 1.** TG curve of $Rb_2Ga_9(PO_4)_8(HPO_4)(OH)F_6·2N_2C_6H_{18}·7H_2O$ (MIL-50) under oxygen gas flow (heating rate 2 °C min^{-1}).

amount of 7 water molecules per $Ga_9(PO_4)_9$ unit (calcd 5.9%). The second weight loss (expt 13.93%) occurring between 200 and 650 °C is attributed to the removal of the organic template (calcd 11%) and the partial removal of fluorine or a hydroxyl group. The third event from 650 °C to 1050 °C is assigned to the departure of the remaining fluorine or hydroxyl group (total weight loss amine + (fluorine, hydroxyl); expt 17.2%, calcd 17.07%). The final decomposition product is a mixture of a dense $GaPO_4$ (low cristobalite form) and an amorphous phase. Powder X-ray thermodiffraction indicates that the structure collapses after the removal of the organic part from 350 °C.

Structure Determination. The structure of MIL-50 was determined by means of single-crystal analysis. A needle-shaped crystal was carefully selected under a polarizing microscope and glued at the top of a thin glass fiber with epoxy adhesive. The intensity data were recorded on a Siemens SMART three-circle diffractometer equipped with a CCD bidimensional detector (molybdenum radiation). The crystal-to-detector distance was 45 mm, allowing for the data collection up to 60° (2θ). Slightly more than one hemisphere of data was recorded, and the acquisition time per frame was 60 s with a scan width of 0.3° in ω. An empirical absorption correction was applied using the SADABS program.[25] MIL-50 structure was solved by direct methods in the noncentric space group $Cmc2_1$ and refined by full-matrix least squares using the SHELXTL package.[26] Gallium and phosphorus atoms were located by direct methods, and all the other non-hydrogen atoms (F, O, C, N) were placed from subsequent Fourier-difference map calculations. Location of fluorine atoms on four crystallographic sites was deduced from analysis of the anisotropic thermal parameters and bond valence calculations. However, the fluorine content obtained from the chemical analysis is slightly lower than expected (5.3% instead of 6.2%), indicating that these four fluorine positions are partially occupied by hydroxyl groups. Hydrogen atoms of amine molecules were placed, at first, with geometrical restraints in the riding mode and refined isotropically. At the final stage, water molecules were located from examination of the Fourier-difference map. For some of them, the occupancy factors were fixed at 50% from thermal parameter values consideration and geometrical constraints because of abnormally short OiW−OjW distances (<2.27 Å). The final refinement converged at R1(F) = 0.0502 and wR2(F^2) = 0.1212 for 3504 reflections [$I > 2\sigma(I)$]. Crystal data and details of the data collection are summarized in Table 1. The resulting atomic coordinates of MIL-50 are listed in Table 2.

NMR Experiments. NMR experiments were run on a DSX 500 Bruker spectrometer with a 11.7 T magnetic field. ^{31}P spectra were obtained at a resonating frequency of 202 MHz. The MAS spectra were

(17) Loiseau, T.; Férey, G. *J. Solid State Chem.* **1994**, *111*, 407.
(18) Loiseau, T.; Férey, G. *J. Mater. Chem.* **1996**, *6*, 1073.
(19) Sassoye, C.; Loiseau, T.; Férey, G.; Taulelle, F. *Chem. Commun.* **2000**, 943.
(20) Sassoye, C.; Marrot, J.; Loiseau, T.; Férey, G. *Chem. Mater.* **2002**, *14*, 1340.
(21) Beitone, L.; Marrot, J.; Lorentz, C.; Taulelle, F.; Loiseau, T.; Férey, G. *Sol. State Sci.* **2001**, *3*, 641.
(22) Beitone, L.; Guillou, O.; Millange, F.; Loiseau, T.; Férey, G. *Sol. State Sci.* **2002**, *4*, 1061.
(23) Lii, K.-H. *Inorg. Chem.* **1996**, *35*, 7440.
(24) Hammond, R. P.; Zubieta, J. A. *J. Solid State Chem.* **1999**, *144*, 442.

(25) Sheldrick, G. M.; SADABS program: Siemens Area Detector ABSorption corrections.
(26) Sheldrick, G. M.; SHELXTL, version 5.03 ed.; Siemens Analytical X-ray Instrument: Madison, WI, 1994.

Table 1. Crystal Data and Structure Refinement for MIL-50

empirical formula	$Rb_2Ga_9(PO_4)_8(HPO_4)(OH)F_6\cdot$ $2N_2C_6H_{18}\cdot7H_2O$
temperature	296(2) K
wavelength	0.71073 Å
crystal system, space group	orthorhombic, $Cmc2_1$
unit cell dimensions	$a = 32.1510(2)$ Å; $\alpha = 90°$
	$b = 17.2290(3)$ Å; $\beta = 90°$
	$c = 10.2120(1)$ Å; $\gamma = 90°$
volume	5656.69(10) Å^3
Z, calculated density	4, 2.461 mg/m^3
absorption coefficient	6.308 mm^{-1}
F(000)	4048
crystal size	$0.50 \times 0.02 \times 0.01$ mm^3
θ range for data collection	1.27−23.28°
limiting indices	$-34 \leq h \leq 35$, $-19 \leq k \leq 17$, $-11 \leq l \leq 11$
reflections collected/unique	12997/4144 [R(int) = 0.0635]
completeness to $\theta = 23.28$	100.0%
absorption correction	SADABS
max and min transmission	0.9396 and 0.1446
refinement method	full-matrix least-squares on F^2
data/restraints/parameters	4144/8/345
goodness-of-fit on F^2	1.161
final R indices [$I > 2\sigma(I)$]	R1^a= 0.0509; wR2^b= 0.1212
R indices (all data)	R1^a= 0.0701; wR2^b= 0.1423
absolute structure parameter	−0.03(2)
extinction coefficient	0.00139(2)
largest diff peak and hole	1.821 and −1.215 e.A^{-3}

^{a} R1 $= \sum||F_o| - |F_c||/\sum|F_o|$. ^{b} wR2 $= \{\sum[w(|F_o|^2 - |F_c|^2)^2]/\sum[w(|F_o|^2)^2]\}^{1/2}$; $w = 1/[\sigma^2(F_o^2) + (0.00778P)^2]$, where $P = [(F_o^2) + 2F_c^2]/3$.

run in a 4 mm MAS probehead. Single pulse MAS, radio frequency driven recoupling (RFDR),[27,28] and double quantum (DQ)[29] experiments were run on phosphorus. The double quantum experiment is obtained by a pulse sequence with two C7 blocks of excitation and reconversion separated by the incremented t1 time.[29] Gallium NMR has been also acquired at high spinning speed (30 kHz) on a 2.5 mm MAS probe from Bruker. The spectrum not fully resolved because of the overlapping of the second order of five inequivalent gallium sites is not shown. Experimental parameters are given in Table 3.

Results & Discussion

Structure Description. The structure of MIL-50, Rb_2Ga_9-$(PO_4)_8(HPO_4)(OH)F_6\cdot2N_2C_6H_{18}\cdot7H_2O$, viewed along [001] shows a three-dimensional framework consisting of channels delimited by 18 and 6 polyhedra (Figure 2). It is built up from the connection by the corner sharing of tetrahedral phosphate groups PO_4 with gallium trigonal bipyramids $GaO_4(F,OH)$ and octahedra $GaO_4(F,OH)_2$ and $GaO_3(F,OH)_3$. All the phosphate oxygen atoms are linked to the gallium atoms except the oxygen O19, which is terminal and coordinated to the phosphorus atom P5 (P5−O19 = 1.556(4) Å). It corresponds to the hydroxyl group of an HPO_4 unit. The phosphate groups have a regular tetrahedral configuration with P−O distances ranging from 1.510(3) to 1.556(4) Å and O−P−O angles close to 109°. Two-thirds of the gallium atoms are 5-fold coordinated to four oxygen atoms and one fluorine/hydroxyl group. The resulting trigonal bipyramid is distorted along the axial direction. The three short Ga−O distances of the trigonal plane are in the range 1.845(2)−1.866(2) Å, whereas the two Ga−O and Ga−(F,OH) apical distances are longer with Ga−O = 1.945(2)−1.965(2) Å and Ga−(F,OH) = 1.945(2)−2.056(2) Å. The remaining gallium

(27) Sun, B. Q.; Costa, P. R.; Kocisko, D.; Lansburgy, P. T., Jr.; Griffin, R. G. *J. Chem. Phys.* **1995**, *102*, 702.
(28) Sun, B. Q.; Costa, P. R.; Griffin, R. G. *J. Magn. Reson. A* **1995**, *112*, 191.
(29) Lee, Y. K.; Kurur, N. D.; Helmle, M.; Johannessen, O. G.; Nielsen, N. C.; Levitt, M. H. *Chem. Phys. Lett.* **1995**, *242*, 304.

Table 2. Atomic Coordinates ($\times10^4$) and Equivalent Isotropic Displacement Parameters (Å$^2 \times 10^3$) for MIL-50

	x	y	z	U(equiv)^a
Rb(1)	3348(1)	4273(1)	9605(1)	67(1)
Ga(1)	806(1)	736(1)	7889(1)	13(1)
Ga(2)	2431(1)	882(1)	7992(1)	12(1)
Ga(3)	1684(1)	1771(1)	11 073(1)	13(1)
Ga(4)	2748(1)	2369(1)	11 323(1)	12(1)
Ga(5)	0	509(1)	12 127(1)	13(1)
P(1)	2451(1)	626(1)	11 046(1)	12(1)
P(2)	3417(1)	3154(1)	13 162(1)	12(1)
P(3)	910(1)	678(1)	10 957(1)	13(1)
P(4)	2031(1)	2704(1)	13 347(1)	11(1)
P(5)	0	1274(1)	6625(2)	17(1)
F(1)	2339(1)	1495(1)	6288(2)	19(1)
F(2)	411(1)	−73(1)	8316(2)	34(1)
F(3)	2213(1)	2316(1)	10 422(2)	19(1)
F(4)	0	1469(2)	13 085(3)	28(1)
O(1)	2424(1)	2295(1)	12 928(3)	15(1)
O(2)	2779(1)	1262(1)	11 264(3)	14(1)
O(3)	2554(1)	20(2)	6991(3)	20(1)
O(4)	3076(1)	2518(1)	9755(2)	15(1)
O(5)	3241(1)	2478(1)	12 358(3)	16(1)
O(6)	2466(1)	310(1)	9653(2)	11(1)
O(7)	2924(1)	1407(1)	8200(2)	14(1)
O(8)	3105(1)	3826(1)	13 368(2)	16(1)
O(9)	1050(1)	623(1)	9517(3)	15(1)
O(10)	1659(1)	2447(2)	12 474(3)	17(1)
O(11)	1170(1)	1283(1)	11 648(2)	14(1)
O(12)	450(1)	893(1)	11 048(3)	19(1)
O(13)	1203(1)	1544(1)	7431(2)	18(1)
O(14)	1006(1)	130(1)	6538(2)	18(1)
O(15)	1458(1)	2152(1)	9529(2)	14(1)
O(16)	2005(1)	889(1)	11 390(3)	18(1)
O(17)	0	−453(2)	11 062(4)	17(1)
O(18)	386(1)	1438(2)	7468(3)	27(1)
O(19H)	0	1866(3)	5475(4)	39(2)
N(1)	2033(1)	3837(2)	9264(3)	22(1)
C(1)	1644(1)	4125(3)	9869(5)	48(1)
C(2)	1409(2)	4700(3)	9028(7)	161(4)
C(3)	1087(2)	5221(3)	9663(10)	313(9)
C(4)	902(3)	5969(4)	9194(6)	393(13)
C(5)	715(4)	6071(4)	10 533(6)	409(13)
C(6)	785(3)	6809(3)	11 282(7)	245(7)
N(2)	994(2)	7417(3)	10 500(6)	127(3)
O(1W)^b	0	2345(6)	9915(12)	171(4)
O(2W)	656(3)	2421(5)	12 929(13)	244(4)
O(3W)^b	0	3810(20)	7600(40)	168(15)
O(4W)^b	637(4)	2901(8)	10 007(15)	156(5)
O(5W)^b	0	3910(20)	9820(40)	155(15)

^{a} U(equiv) is defined as one-third of the trace of the orthogonalized **U**ij tensor. ^{b} Occupancy factor 50%.

atoms are octahedrally coordinated with typical Ga−O and Ga−(F,OH) distances in the range 1.911(2)−1.983(3) Å. Ga4 is connected to four oxygens and two fluorine/hydroxyl groups, whereas Ga5 is linked to three oxygen atoms and three fluorine/hydroxyl groups. For the latter, one of the fluorine sites (F4) is terminal with a shorter Ga5−F4 = 1.921(3) Å and should be fully occupied by fluorine. Such a situation was previously observed in the gallium fluorophosphates GaPO$_4$−CJ2,[30] pseudo-KTP,[31] or MIL-46[20] networks in which short terminal Ga−F bonds (1.88−1.90 Å) occur. The other fluorine/hydroxyl groups are in a bridging position between two gallium atoms with Ga−(F,OH) distances of 1.945(2)−1.978(2) Å.

The inorganic framework is composed of two closely related structural building units comprising three phosphates groups and

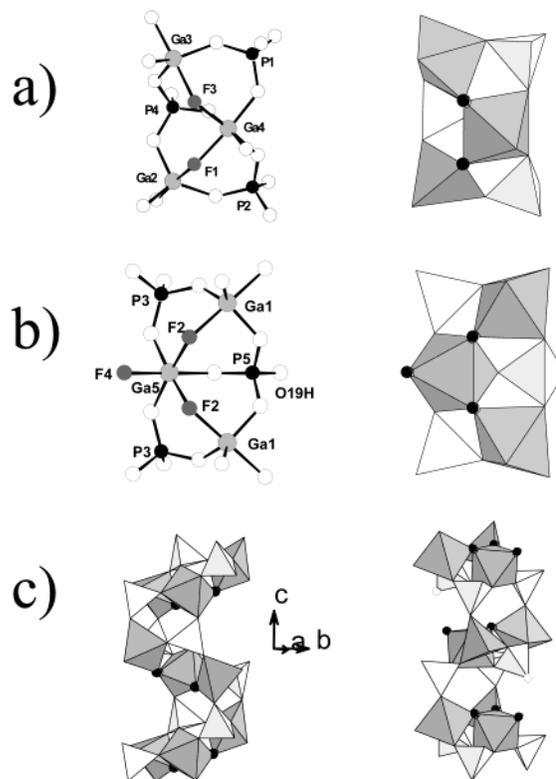(30) Férey, G.; Loiseau, T.; Lacorre, P.; Taulelle, F. *J. Solid State Chem.* **1993**, *105*, 179.
(31) Loiseau, T.; Paulet, C.; Simon, N.; Munch, V.; Taulelle, F.; Férey, G. *Chem. Mater.* **2000**, *12*, 1393.

Table 3. NMR Parameters of Acquisition

^{31}P measurement conditions for RFDR	
spectrometer	DSX500 Bruker (11.7 T)
probe	MAS 4 mm H-X Bruker
spinning frequency	12.5 kHz
^{31}P radio frequency fields	202.414 MHz
mixing time	96 ms
sweep width 1	6250 Hz
sweep width 2	6250 Hz
recycle delay	2 min
t90 pulse length	3.44 μs
scan number	16
t1 increment	80 μs
number of increments	49
reference used	(NH$_4$)H$_2$PO$_4$ (δ = 0 ppm)
^{31}P measurement conditions for C7	
spectrometer	DSX500 Bruker (11.7 T)
probe	MAS 4 mm H-X Bruker
spinning frequency	11074 Hz
^{31}P radio frequency fields	202.414 MHz
excitation/reconversion time	361.2 ms
sweep width 1	5537.1 Hz
sweep width 2	9689.92 Hz
recycle delay	100 s
t90 pulse length	2.98 μs
scan number	32
t1 increment	90.30 μs
number of increments	41
reference used	(NH$_4$)H$_2$PO$_4$ (δ = 0 ppm)
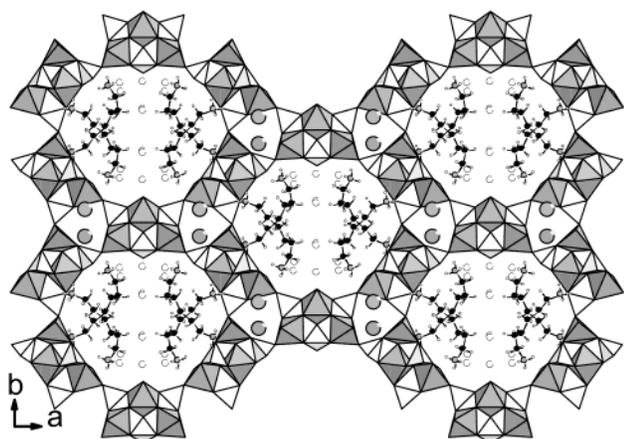
Figure 2. View of the structure of MIL-50 along the *c* axis showing the 18-ring channels. White polyhedra, phosphorus groups; gray polyhedra, gallium; open circles, water molecules; large gray circles, rubidium; black circles, carbon; gray circles, nitrogen; small open-circles, hydrogen.

three gallium centers (Figure 3). Two 5-fold coordinated gallium atoms are linked to one octahedral gallium atom via the fluorine/hydroxyl groups located in cis position. This gallium trimer is connected to the three phosphates by a corner and forms a Ga$_3$P$_3$ species. This type of building unit is commonly encountered in the fluorinated gallium phosphate family exhibiting layered structures (ULM-8,[32] DAO−GaPO,[18] MIL-30[33]) or three-dimensional frameworks (ULM-3,[18] ULM-4,[34] ULM-5,[17] ULM-16,[18] TREN-GaPO,[7] MIL-31,[19] MIL-46[20]). The two asymmetric units differ only by the presence of the terminal atom: one oxygen O19 attached to the phosphorus P5 and one fluorine F4 attached to the gallium Ga5. This specific configuration

(32) Serpaggi, F.; Loiseau, T.; Riou, D.; Férey, G.; Hosseini, M. W. *Eur. J. Solid State Inorg. Chem.* **1994**, *31*, 595.
(33) Paulet, C.; Loiseau, T.; Férey, G. *J. Mater. Chem.* **2000**, *10*, 1225.
(34) Loiseau, T.; Taulelle, F.; Férey, G. *Mic. Mat.* **1997**, *9*, 83.

Figure 3. Representation of the building species: (a) hexameric building unit [Ga$_3$(PO$_4$)$_3$(F,OH)$_2$]; (b) hexameric building unit [Ga$_3$(PO$_4$)$_2$(HPO$_4$)(F,OH)$_2$F]; (c) connection mode of the file of the hexamers [Ga$_3$(PO$_4$)$_3$(F,OH)$_2$] along the *c* axis (left), and the hexamers [Ga$_3$(PO$_4$)$_2$(HPO$_4$)(F,OH)$_2$F] (right). For the polyhedral representations, the fluorine atoms and hydroxyl groups are indicated by black circles and open circles, respectively.

occurs for one-third of the building species and corresponds to the formulation [Ga$_3$(PO$_4$)$_2$(HPO$_4$)(F,OH)$_2$F]. Because of the presence of terminal atoms, it results in these hexameric building units being linked to each other through two connection points (Figure 3) along the *c* axis (P−O−Ga bonds). A distance of 2.535(5) Å is observed between the terminal fluorine atom F4 and terminal oxygen atom O19. In pseudo-KTP,[31] a similar situation was found with an identical nonbonding atoms O···F distance of 2.50 Å. For the other two-thirds of building units, [Ga$_3$(PO$_4$)$_3$(OH,F)$_2$], the connection along the *c* axis occurs through three Ga−O−P nodes, as represented in Figure 2. This arrangement mode is identical to that observed in the other gallium phosphates on the basis of the hexameric building brick [Ga$_3$(PO$_4$)$_3$F$_2$]. The files of these building units are connected together in order to generate a layer in the (*a*,*b*) plane. These hexamer sheets are linked through the other type of asymmetric unit [Ga$_3$(PO$_4$)$_2$(HPO$_4$)(F,OH)$_2$F], and a three-dimensional network with large channels with 18 rings running along the *c* axis are formed. The free pore diameter is 10.9 × 9.1 Å (on the basis of an oxygen ionic radius of 1.35 Å).

The 1,6-diaminohexane molecules are located within the 18-ring tunnels, and the terminal nitrogen atoms point toward the mineral framework. The diamine is protonated, and the ammonium groups preferentially interact with the anions (O, F) of the building unit [Ga$_3$(PO$_4$)$_3$(F,OH)$_2$] via hydrogen bonds. As usually observed in this class of solids, hydrogen bond interactions occur between the bridging fluorine/hydroxyl groups (F1 and F3) and one of the ammonium groups (N1−H1C···F1

a

b
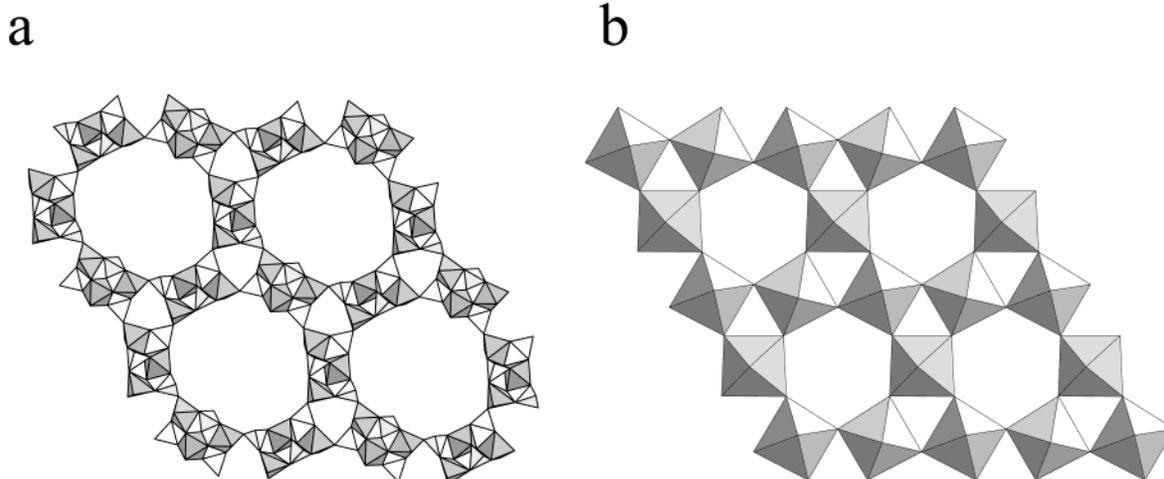
Figure 4. Topological analogy between (a) MIL-50 and (b) K_xWO_3.

= 2.076(2) Å, N1−H1B···F3 = 2.451(2) Å). The other ammonium head is linked with oxygen atoms belonging to the network (N2−H2E···O13 = 1.920(2) Å). Some water molecules are also encapsulated within the 18-ring pores and interact mainly with the ammonium groups (N2−H2C···O2W = 1.989(13) Å) and anions of the second type of hexameric unit $[Ga_3(PO_4)_2(HPO_4)(F,OH)_2F]$.

The rubidium atoms reside in the 6-ring channels running along the *c* axis and are coordinated to 10 oxygen atoms and 1 fluorine/hydroxyl group (F1). The Rb−O distances are within 3.027(3)−3.676(3) Å, and the Rb−(OH,F) distance is 3.097(2) Å (Figure 5). The locations of the alkaline cations are identical to those of water molecules present within the 6-ring channels of the other 18-ring gallium phosphates MIL-31[19] and MIL-46.[20] The positive charges of two rubidium cations (+2) and two diprotonated 1,6-diaminohexane (+4) balance the negative part of the inorganic framework $[Ga_9(PO_4)_8(HPO_4)(OH)F_6]$.[6−]

The TGA experiment gives a total amount of 7 water molecules per Ga_9P_9 unit, although the XRD analysis indicates the positions of 4.5 water molecules. The other "liquid water" molecules are probably localized in the region where the OiW sites are fractionally occupied. The several sites with fractional occupancy would indicate that these unobserved molecules are jumping back and forth between the possible sites, leaving there only a fraction of their electronic density.

Units and Topology. The topology of MIL-50 is close to that encountered in the tungstate oxide K_xWO_3 with the hexagonal bronze structure type.[35] The Ga_3P_3 hexameric species of the MIL-50 framework can be considered as the equivalent WO_6 octahedral units present in the tungstate. The arrangement of these units is identical for both networks (Figure 4) except the existence of P−OH and Ga−F terminal bonds, which distort the MIL-50 topology from the hexagonal symmetry. The observation is a nice illustration of the concept of scale chemistry developed by Férey.[36] For a given building brick (octahedral unit MO_6 or hexamer Ga_3P_3), their connection mode is identical. Only the metric of the cavity differs because of the actual size of the building unit. This fact was also observed in the series of porous metal organic carboxylates synthesized by
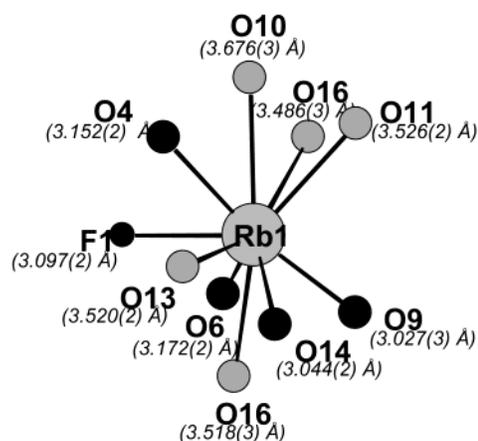
(35) Magneli, A. *Acta Chem. Scand.* **1953**, *7*, 315.
(36) Férey, G. *J. Solid State Chem.* **2000**, *152*, 37.

Figure 5. $RbO_{10}(F,OH)$ connexity up to 3.7 Å and details of the Rb anion distances. For easier readability, atoms within 3.2 Å have been blackened and atoms between 3.2 and 3.7 Å grayed.

Yaghi and co-workers.[37] In these solids, the porosity is controlled by the geometry of the secondary building unit (tetrahedron, square plane, cube, etc.) of the metallic cluster and the size and conformation of the organic carboxylates acting as linkers. The arrangements of these building blocks are related to those of basic structure types (diamond, quartz, rutile, fluorite, etc.).[38]

Assembling of Hexameric Units. The structure of MIL-50 is a third example of fluorinated gallium phosphate three-dimensional frameworks containing 18-ring channels. Previously, this specific feature was reported in two other gallophosphates MIL-31[19] and MIL-46.[20] In these three solids, the framework is interrupted because of the presence of terminal anions attached to the metal atoms (P or Ga), preventing a complete Ga−O−P connection. These compounds are characterized by the existence of identical building species $[Ga_3(PO_4)_3F_2]$, which are connected in the same manner by forming sheets of hexamers Ga_3P_3. In these planes, the cell parameter corresponding to the stacking of two building units $[Ga_3(PO_4)_3F_2]$ is identical with a periodicity of ~10.2 Å. It is

(37) Eddaoudi, M.; Moler, D. B.; Li, H.; Chen, B.; Reineke, T. M.; O'Keeffe, M.; Yaghi, O. M. *Acc. Chem. Res.* **2001**, *34*, 319.
(38) O'Keeffe, M.; Eddaoudi, M.; Li, H.; Reineke, T.; Yaghi, O. M. *J. Solid State Chem.* **2000**, *152*, 3.

also a common value for other hexamer-based gallium phosphates (ULM-3,[39] ULM-4,[34] ULM-5,[17] ULM-8,[32] ULM-16[18]). The linkage between the hexamer layers is ensured by the addition of another building unit with a different configuration, which generates the 18-ring 1D tunnel network. The existence of an extra large 18-ring pore is not specific to the fluorinated gallium phosphate series, since the purely tetrahedral network of aluminophosphate VPI-5[40] also possesses an 18-ring channel system with the same topology. MIL-50 is therefore equivalent to VPI-5 but with nontetrahedrally coordinated atoms.

Volume Analysis. The framework density (FD, number of the metal atoms P and Ga per unit volume) of such a topology is 12.7 T atoms/1000 Å^3 and is comparable with those of other gallium phosphate series with 18-ring pores (MIL-31,[19] FD = 12.6; MIL-46[20] = 12.0). It is equivalent to the value found in the aluminosilicate faujasite[41] (12.7) and slightly higher to that of the gallium phosphate cloverite[5] (11.1) containing a 3D system of 20-ring channels. By ignoring the structure-directing agent and water molecules trapped within the 18-ring pores, we can estimate the fraction of the unit cell volume corresponding to the framework by using the CALC SOLV option in the program PLATON.[42] The volume for the potential access of "solvent molecules" is worked out on the basis of occupancy of the atoms (van der Waals radii) of the mineral framework (Ga, P, O, F, Rb). The calculations indicate that 2378 Å^3 per unit cell or 42% of the cell volume might be accessible if the inserted species are removed.

Rubidium Case. The rubidium cation seems to play a critical role for the formation of the 18-ring open-framework MIL-50 synthesized with 1,6-diaminohexane as the structure-directing agent. The use of this organic species was already reported for the GaPOF compound ULM-5.[17] It exhibits a three-dimensional network delimiting 16-ring tunnels and was obtained with the same diamine. ULM-5 and MIL-50 frameworks are closely related and differ by the existence of a cubic building unit (D4R type) in ULM-5 instead of a hexameric unit in MIL-50. A comparison of ULM-5 and MIL-50 phases indicates that rubidium atoms (MIL-50) and water molecules (ULM-5[17]) are located within the 6-ring channels. The diamine is present within the larger pores for both structures and is the key parameter for the formation of extra large pores. However, the positive charge of rubidium modifies the electroneutrality of the system and therefore leads to a novel topology. In this phase, the rubidium acts as a supplementary charge compensator, which induces a new configuration of building unit arrangement. This configuration was not observed for other amines in similar open frameworks[56] (ULM-3, TREN-GaPO) produced in the presence of rubidium. In these latter cases, the rubidium atoms replace partially the organic molecules without any structure modification. Here, the rubidium cation is tightly corseted by the oxygen atoms belonging to the two 6-rings tunnels. This rubidium tight protection impedes the solvation of the cation and reinforces the connection of the three hexameric units. This situation is unique, since, in the hydrated compounds incorporating alkaline cations, the occluded water molecules usually belong to the coordination sphere of the alkaline cations.
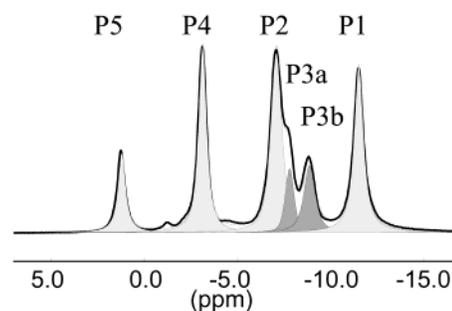

Figure 6. MAS ^{31}P NMR of MIL-50. MAS spinning speed 10 kHz, spectrum and decomposition. Components corresponding to XRD multiplicity are light gray, and the component having a higher multiplicity than in XRD is dark gray.

Different attempts of cationic exchange of rubidium by smaller alkaline cations were undertaken. These experiments were carried out from a mixture of LiCl or NaCl solution and a powdered sample of MIL-50, but they revealed that the rubidium cations still remain within the open-framework solid.

^{31}P NMR Structural Aspects. High-resolution solid-state NMR is efficient to reveal structural information of crystalline materials. Experimental schemes such as SEDRA,[43] RFDR,[27,28,44] DRAMA,[45,46] HORROR,[47] and C7[29] have allowed the recovery of the homonuclear dipolar interaction, while, in MAS, these schemes present all different characteristics as well as different domains of applicability. These make possible, in numerous cases, the study of the local topology of materials by considering the atomic through-space connexities.[48] In this study, we used ^{31}P 2D RFDR & double-quanta experiments (DQ), to elucidate the topology of the phosphorus sublattice.

The MAS ^{31}P spectrum (Figure 6) exhibits six different signals. To ensure that all these sites do belong to the same phase and not to a mixture of phases, an RFDR experiment has been obtained with very long mixing times. It appears that all sites are dipolarly coupled or reachable via spin diffusion, leading therefore to all phosphorus sites having cross-peaks with every other site. The phase is therefore a pure phase, and further reasoning can be carried between XRD on single crystal and NMR on powder with the knowledge that the same object is actually considered.

The site population ratio is 1:2:2:1:1:2, whereas the XRD single-crystal structure analysis leads to a 1:2:2:2:2 population ratio. One can assign the inequivalent phosphorus atoms by using a relation between an isotropic quantity, the mean ⟨PO⟩ distance or the mean ⟨POGa⟩ angle of the isotropic chemical shift. The latter correlation seems to be more accurate in the case of small differences than the first.[49,50] In this case, the mean ⟨POGa⟩ versus isotropic chemical shift correlation is definitely linear (Figure 7) and allows empirical assignments between XRD and NMR inequivalent sites. The mean ⟨POGa⟩ angles are ranked by increasing values of 122.0, 127.7, 132.0, 133.7,

(39) Loiseau, T.; Retoux, R.; Lacorre, P.; Férey, G. *J. Solid State Chem.* **1994**, *111*, 427.
(40) Davis, M. E.; Saldarriaga, C.; Montes, C.; Garces, J.; Crowder, C. *Nature* **1988**, *331*, 698.
(41) Baur, W. H. *Am. Mineral.* **1964**, *49*, 697.
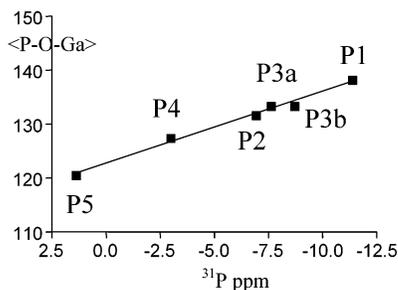(42) Spek, A. L. Utrecht University: Utrecht, The Netherlands, 2001.
(43) Bennett, A. E.; Ok, J. H.; Griffin, R. G.; Vega, S. *J. Chem. Phys.* **1992**, *96*, 8624.
(44) Baldus, M.; Tomaselli, M.; Meier, B. H.; Ernst, R. R. *Chem. Phys. Lett.* **1994**, *230*, 329.
(45) Tycko, R.; Dabbagh, G. *J. Am. Chem. Soc.* **1991**, *113*, 9444.
(46) Tycko, R.; Smith, S. O. *J. Chem. Phys.* **1993**, *98*, 932.
(47) Nielsen, N. C.; Creuzet, F.; Griffin, R. G.; Levitt, M. H. *J. Chem. Phys.* **1992**, *96*, 5668.
(48) Munch, V.; Taulelle, F.; Loiseau, T.; Férey, G.; Cheetham, A. K.; Weigel, S.; Stucky, G. D. *Magn. Reson. Chem.* **1999**, *37*, S100.
(49) Sternberg, U.; Pietrowski, F.; Priess, W. *Z. Phys. Chem.* **1990**, *168*, 115.
(50) Sternberg, U.; Koch, F. T. *Comput. Chem. Proc. 5* **1991**, 183.

Figure 7. ⟨POGa⟩ means angle versus ^{31}P isotropic chemical shift (in ppm versus H_3PO_4).

and 137.8 and lead to a P5, P4, P2, P3, and P1 order when considering the radio-crystallographic labeling. When ranking chemical shifts, one observes 1.18, −3.16, −7.11, −7.83, −8.89, and −11.54 ppm versus H_3PO_4 85%. P3 is, therefore, the phosphorus site that is split in NMR versus XRD (noted P3a and P3b in Figure 6). The remaining phosphorus inequivalent sites have a consistent multiplicity between XRD and NMR. To confirm this assignment, a double quantum (DQ) experiment has been performed. It is displayed on Figure 8 and is completely consistent with the assignment given previously. One must notice, however, weak cross-peaks for all phosphorus sites that are in the vicinity of P3. These weak intensities will be discussed later. But, even with this observation in mind, the assignment obtained by the analysis of the DQ is not different from the one deduced from MAS, multiplicity analysis, and empirical correlation of chemical shifts and mean angles.

However, the multiplicity of the phosphorus site P3 observed by diffraction analysis and ^{31}P NMR differs. The diffraction experiment gives a multiplicity of two for P3 compared to P5, but a twice multiplicity of one is observed by NMR. Additionally, for NMR, P3 only is affected by the multiplicity modification.

The examination of the structure indicates that the phosphorus atoms P3 belong to the second type of hexameric unit $[Ga_3(PO_4)_2(HPO_4)(F,OH)_2F]$. It consists of two inequivalent phosphorus atoms P3 and one P5 with two distinct multiplicities (P3/P5 ratio of 2/1). Two phosphate groups (P3) are located on the corners of the unit, and one (P5) is in the middle. This building block faces the water molecules encapsulated within the large 18-ring channels. The different water molecules are located in a confined space limited by the hydrophobic part of the 1,6-diaminohexane species and the inorganic "walls" of the 3D framework. Nevertheless, within this XRD structural analysis, it appears that environments of the two phosphorus atoms P3 of the hexameric unit are identical. Each P3 interacts symmetrically with the same water molecules or ammonium groups of the diamine. This structural model does not reflect the ^{31}P NMR measurement, since the resonance signal assigned to P3 is split into two equal components. To further the consequences of these results, one must propose a better structural model where water molecules and hydrogen atoms are localized.

Completing the Structural Model of MIL-50 with Hydrogens and Water. Extensive intermolecular H bonding with the surrounding medium smears out the electronic density, creating difficulties in localizing hydrogen atoms by XRD. Therefore, another method has been used to provide the localization of H atoms in water molecules and hydroxo and ammonium groups

commonly encountered in microporous compounds. Its principle is to treat H-atom coordinates as adjustable parameters during the minimization (amoebae downhill simplex algorithm) of the Madelung lattice energy of the crystal. The critical point in this technique lies in the fast and reliable evaluation of the atomic charge distribution directly from each atomic position set, the possible crystal structure, generated at each amoebae move. Such high-quality partial charge distributions are obtained using the nonempirical form of the PACHA model,[51−54] known to lead hydrogen atomic coordinates in very good correlation with those derived from neutron diffraction data.[55] However, to perform these Madelung summations, the crystallographic data must be reshaped in a general standard format.

First, for centered lattices, a unit cell transformation leading to a primitive cell must be applied. If this step is not mandatory, it reduces considerably the computation time needed for the evaluation of the Madelung matrix, because of the unit cell reduction by a factor of 2, 3, or 4, depending on the space group. Thus, in the case of MIL-50 (76 atoms in the asymmetric unit cell), a standard crystallographic transformation from the centered unit cell to the primitive unit cell of the $Cmc2_1$ space group has been performed. This new setting of space group $Cmc2_1$ (space group number 36 with primitive unit cell) is labeled hereafter as $pmc2_1$ to avoid confusion with $Pmc2_1$ (space group number 26) and is characterized by the following parameters: $a = b = 18.238$ Å, $c = 10.212$ Å, $\alpha = \beta = 90°$, $\gamma = 56.37°$. With this transformation, the size of the Madelung matrix has been reduced from 152×152 (space group $Cmc2_1$) down to 76×76 (space group $pmc2_1$).

The second step concerns the atoms displaying full occupancy factors but missing H-atom coordinates, such as N1 (3H), N2 (3H), O2W for MIL-50, while hydrogen positions of CH_2 were not redetermined. Here, extra chemical knowledge not contained in the X-ray diffraction experiment should be added. In the present case, for the six H atoms around atoms N1 and N2, N−H bond lengths were fixed at 1.05 Å and C−N−H or H−N−H bond angles were fixed at 110° (tetrahedral geometry around nitrogen). For each of the two NH_3 groups, two dihedral angles were also kept fixed at ±120°. The two last dihedral angles were allowed to take any arbitrary value between 0 and 360°. Similarly, two H atoms were added around atom O2W using two O−H bond lengths of 0.97 Å and an H−O−H bond angle fixed at 105°. The three other angles were, as before, allowed to take any arbitrary value between 0 and 360°. These adjustable parameters define the first five vertexes of the MIL-50 simplex search.

The third step is the most delicate, as it concerns atoms having partial occupancy factors. As we want to obtain a structural model that is fully compatible with a chemical analysis, full occupancy factors must be obtained. This has the following implication. The unit cell must be divided into several sublattices, each of them being described by a different space group. The "cocrystal" thus obtained may allow for such a coexistence of several space-group symmetries within the same unit cell. The general procedure to do this is to define for each atomic

(51) Henry, M. *Mater. Sci. Forum* **1994**, *152−153*, 355.
(52) Henry, M. *Top. Mol. Organ. Eng.* **1997**, *15*, 273.
(53) Henry, M. *Coord. Chem. Rev.* **1998**, *178−180*, 1109.
(54) Henry, M. *ChemPhysChem* **2002**, *3*, 561.
(55) Henry, M. *ChemPhysChem* **2002**, *3*, 607.
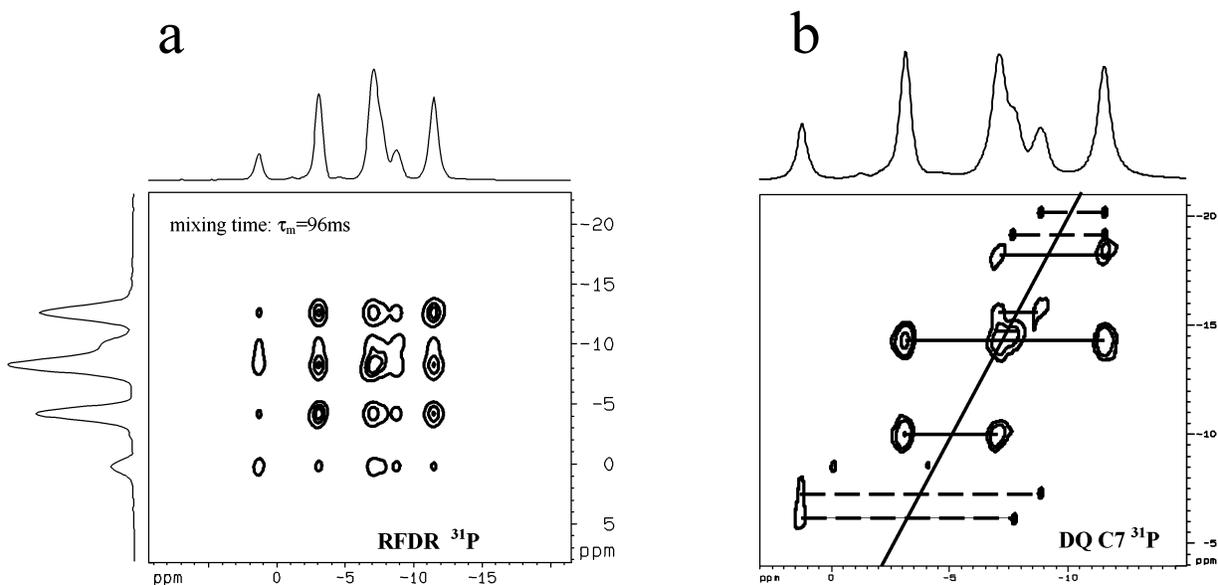(56) Beitone, L.; Marrot, J.; Loiseau, T.; Férey, G. *Mic. Mes. Mat.* **2002**, *56*, 163.

Figure 8. ^{31}P NMR (a) RFDR and (b) DQ C7 (see conditions in the text) cross-peaks in black are highlighted to visualize them on the contour plot despite their low intensity. Continuous lines connect the cross-peaks that can be located by visual inspection of the contour plot only; dashed lines connect cross-peaks detected by inspection of the corresponding slices.

site displaying partial occupancy factors a symmetry mask. This symmetry mask is formed from a reduced number n ($n < 4$) of symmetry operations belonging to the $pmc2_1$ group. Let us notice that the choice of the symmetry operations, which should be removed for a given site, is not arbitrary but is dictated again by chemical knowledge, not derived from the X-ray diffraction measurement. Here, the additional information needed to go one step further in the description of the structural model as a cocrystal is the same as what has been already used in step two, with a supplementary constraint that two O atoms separated by less than 2.4 Å in distance is a very unlikely situation and therefore must be rejected. The MIL-50 structure is a perfect example of this structural model description, which may be applied to produce realistic structural models starting from the disordered first approximation derived from single-crystal X-ray measurement. As the space group order of $pmc2_1$ is 4, symmetry masks can be defined only for atoms displaying occupancy factors 0, $^1/_4$, $^1/_2$, or 1. The four symmetry operations for $pmc2_1$ being identity (#1 = $x,y,z \rightarrow x,y,z$), 2_1 screw-rotation along the c-axis (#2 = $x,y,z \rightarrow -x,-y,^1/_2+z$), $c(x,x,z)$ glide plane (#3 = $x,y,z \rightarrow y,x,^1/_2+z$), and $m(x,-x,z)$ mirror plane (#4: $x,y,z \rightarrow -y,-x,z$), one starts either from the 1-occupation mask [1234] or from the 0-occupation mask [....]. For $^1/_2$ occupation, six masks may be defined: [12..], [1.3.], [1..4], [.23.], [.2.4] or [..34], while four masks ([1...], [.2..], [..3.], and [...4]) are available for $^1/_4$ occupation. In each mask, a dot means that the corresponding symmetry operation should not be applied during the Madelung summation process. This ensures that only fully neutral stoichiometric unit cells are considered. However, occupancy factors being independently refined during crystal structure determination, it may be possible that some atoms do not fit easily in the (0, $^1/_4$, $^1/_2$, or 1) pattern of space group $pmc2_1$. For instance, in MIL-50, we have assumed that all the sites assigned to fluorine with a partial occupancy of F and OH were occupied by fluorine only. This is obviously an approximation, but it appears to be the simplest one at this level. The validity of such an assumption will be checked a posteriori by its compatibility with NMR data. In the following, we will describe

how symmetry masks may be derived for atoms O1W, O3W, O4W, and O5W, which all display a 50% occupancy factor. In a second step, we will add H atoms to finish up building the structural model.

A good idea is to start with the identity operator and one atom in a special position, for instance O1W(#1). Because of the situation of this atom being on a mirror plane, the starting mask is [12..]. Immediately, two unrealistic short contacts at 2.26(1) Å with O4W(#1) and O4W(#4) are observed. Consequently, applying the [.23.] mask to O4W will avoid this situation. Now, if we keep O4W(#2) and O4W(#3), two other short contacts at 2.26(1) Å with O1W(#2) are still present. Consequently the (O1W[1...], O4W[.23.]) is a "good" combination which ensures the systematic absence of these 2.26(1) Å short contacts. Obviously, by symmetry the (O1W[.2..], O4W[1..4]) combination is an equally "good" possible alternative which should lead to similar results. Let us now turn to the remaining pair (O3W, O5W). Their starting mask is [12..], as both atoms lie on a mirror plane. Since it is known that atom O3W(#1) makes a very short contact at 2.27(6) Å with O5W(#1), it follows that if one choose the [1...] mask for O3W, the mask for O5W should be [.2..]. Again, by symmetry (O3W[.2..], O5W[1...]) is also a "good" combination, avoiding these short contacts. We eventually retained for this study the (O1W[1...], O4W[.23.]) and (O3W[1...], O5W[.2..]) combinations.

With no more unrealistic overlaps between O atoms, it is now possible to define masks for H atoms. The first problem is encountered with O19H, which lies on a mirror plane. Adding one H atom (H66) in general position to this atom using an O–H bond length of 0.97 Å, a P–O–H bond angle fixed at 110°, and a variable dihedral angle leads to the generation of four H atoms instead of two. However, this situation is easily solved by applying a $p2_1$ subgroup constraint ([12..] symmetry mask) to this hydrogen atom and implies a $^1/_2$ occupancy factor. At this stage, the MIL-50 simplex has an additional sixth vertex corresponding to the dihedral angle of atom H66. Adding two H atoms to O1W, O3W, and O5W is a straightforward process,

as only one symmetry operation has to be considered in each case leading to a *P*1 subgroup constraint ([1...] symmetry mask) for these six atoms. As for O2W, the six O−H bond lengths are taken as equal to 0.97 Å and the three H−O−H bond angles are assumed to be 105°. This leaves 9 adjustable angles, increasing the simplex dimension from 6 to 15 vertexes. The remaining two H atoms must be added to O4W. Because of the chosen [.23.] mask, it follows by symmetry that a [1..4] mask (*pm* subgroup constraint) should be applied to these two atoms. With two O−H bond lengths at 0.97 Å and one 105° constraint for the H−O−H bond angle, three remaining angles have to be adjusted leading to a final 18-vertex simplex. At this stage, we have completely removed the apparent "disorder" of the MIL-50 structure using only two extra chemical constraints: removal of the two kinds of very short contacts observed at 2.26(1) and 2.27(6) Å of the original X-ray structural model. As explained previously, these constraints can be expressed in a rigorous way into a symmetry mask pattern for p*mc*2$_1$ space group symmetry.

With a reasonable structural model in hand, charge distributions may be computed at each stage of the simplex algorithm using the following ab initio atomic parameters: (where EN stands for electronegativity, r_{1s}, for the radius of the 1s orbital considered, q, for the fractional charge, and $\langle EB \rangle$, for the electrostatic balance as described in reference[54]) H(EN = 13.610 eV, r_{1s} = 0.53 Å); C(EN = 15.050 eV, r_{2s} = 0.62 Å); N(EN = 18.130 eV, r_{2s} = 0.521 Å); O(EN = 21.360 eV, r_{2s} = 0.45 Å); F(EN = 24.800 eV, r_{2s} = 0.396 Å); P(EN = 13.330 eV, r_{3p} = 0.918 Å); Ga(EN = 10.390 eV, r_{3p} = 1.254 Å), and Rb(EN = 4.177 eV, r_{5s} = 0.990 Å). This last radius for the rubidium atom was dictated by applying the constraint q(Rb) = +1 at each stage of the refinement. Starting from $\langle EB \rangle$ = −36 332.1 kJ mol^{-1}, we observed that our 18-vertex simplex converged after 654 evaluations of the Madelung matrix toward $\langle EB \rangle$ = −36 563.9 kJ mol^{-1}, with a maximum value spotted at $\langle EB \rangle$ = −36 190.5 kJ mol^{-1}. At this stage, we have in hand an optimized geometry describing a cocrystal in which the framework has a rigorous p*mc*2$_1$ space group symmetry and faces water molecules displaying intimately mixed *P*1, *pm*, and *p*2$_1$ space group symmetries. The next step is then to find a common subgroup for all these atoms, and here, the only possibility is *P*1. This is the reason final atomic coordinates including H atoms obtained in space group *P*1 are reported in the CIF file provided in the Supporting Information. Working in the *P*1 space group presents also the net advantage of not making any a priori assumption about the presence or absence of point-group symmetry elements in the crystal. Consequently, at this stage, only pure translation symmetry operations of the full unit cell are operative. This is a legitimate assumption because we are considering a crystal and therefore crystalline lattices sharing the same translational parameters. When other symmetry elements (rotation axes or mirrors) are concerned, they will emerge by themselves after the resulting charge distribution is looked at using a fixed charge difference threshold. This charge difference threshold should not be arbitrary but rather should be fixed after a careful evaluation of all the possible sources of errors. A first, an obvious factor limiting the accuracy of the charge distribution is the number of significant figures used for atomic coordinates. As this study involves five digits for atomic coordinates, differences less than 10^{-5} are meaningless. A second step is to

Table 4. Partial Charges of the Phosphorus Atoms Calculated in the *P*1 Space Group for MIL-50[a]

atom	charge
P1(#1)	+0.535
P1(#2)	+0.534
P1(#3)	+0.534
P1(#4)	+0.534
P2(#1)	+0.533
P2(#2)	+0.534
P2(#3)	+0.534
P2(#4)	+0.533
P3(#1)	+0.531
P3(#2)	+0.533
P3(#3)	+0.533
P3(#4)	+0.531
P4(#1)	+0.520
P4(#2)	+0.520
P4(#3)	+0.520
P4(#4)	+0.520
P5(#1)	+0.554
P5(#2)	+0.553

[a] The partial charge values are obtained using the PACHA method.

take into account that besides atomic coordinates, X-ray analysis provides atomic displacement parameters (ADP). The last digit of atomic coordinates should therefore be considered only as an average over several equally probable possibilities. A simple way to account for these sources of errors on the charges is to consider only meaningful differences lying 1 order of magnitude above the previous accuracy threshold. Consequently, for MIL-50 our charge difference threshold should be at least 10^{-4}. A last, errors stem from assumptions made to generate a reasonable stoichiometric and periodic unit cell, selecting adequate symmetry masks (vide supra). For MIL-50, these causes of errors are listed as the following:

(i) No OH groups are retained on fluorine sites. Partial substitution of fluorine by hydroxo groups on these sites should obviously alter the charge distribution.

(ii) Some water molecules measured by TGA were not localized by X-ray diffraction. Here also, inclusion of the missing water molecules should change the charge distribution, but no effort has been undertaken here in this direction, leaving some room for some uncertainty.

(iii) Finally, our model assumes perfect translation order on the basis of the following selection of symmetry masks: O1W[1...], O3W[1...], O4W[.23.], O5W[.2..]. But an equally valid alternative model would have been the following masks: O1W[.2...], O3W[.2..], O4W[1..4], O5W[1...]. Both are describing equivalent water periodic patterns that are a mirror image of each other. The two charge sets obtained from these two choices are identical. One could therefore think that a crystal is made of only one choice or that any combination of both solutions can occur, leading to polytypes. As we have no evidence of the latter case, we chose one of the two first options, here the first, for the water sublattice.

They do not impact, from previous experience, more than an order of magnitude more than the errors because of atomic position errors, that is, here 10^{-3}. The charge results are given in Table 4 in the case of phosphorus atoms studied by NMR (vide infra). Other atomic charges are available as Supporting Information.

The charge distribution can therefore be taken as a way to analyze the symmetry of the structural model. If the charge difference that a physical measurement can be sensitive to, XRD

or NMR, is coarse (10^{-2}), then charges that lie within this charge difference would be considered identical and the structural model would be described by the highest symmetry, that is, here $pmc2_1$. If the charge difference is definitely too small (10^{-5}), then only $P1$ would be the only way allowed for describing the space group. Between, the charge difference accessible may differentiate only a fraction of inequivalent sites. This is the case for ^{31}P NMR. If a charge difference of 10^{-3} would be significant, then, except P4, all other phosphorus sites would be dedoubled. If the charge difference significant is in the range of 2×10^{-3}, then only P3 is dedoubled. This observation can be directly correlated with the ^{31}P NMR experiment, which shows two resolved resonance peaks for the P3 site only. Actually, all other phosphorus sites must be considered as being dedoubled too, even if this is not detected by this NMR experiment. In such a case, the space group would be Cm (pm), instead of $Cmc2_1$ ($pmc2_1$). Actually, the loss of the 2_1 glide axis, which occurs for the water clusters, implies automatically the loss of the c plane too, leaving only the mirror m as the element of symmetry.

In $pmc2_1$ symmetry, the too short contacts (2.26(1) and 2.27(6) Å) between pairs (O1W, O4W) and (O3W, O5W) would mean a high repulsion between the electronic clouds of the two water molecules, explaining the need for fractional occupancy factors used to analyze the X-ray diffraction results. Modeling this simple avoidance through our symmetry mask approach allows us to handle easily this practical situation. It results that the charge differentiation observed for P3 sites is mainly influenced by the symmetry of the water subnetwork located within the large channels. Actually, because of the symmetry lowering, two water sublattices appear from the structural model described in the space group $P1$. A pattern of five water molecules is present on one side of the hexameric unit [Ga$_3$(PO$_4$)$_2$(HPO$_4$)(F,OH)$_2$F], whereas a pattern of four is observed on the other side (Figure 9).

^{31}P NMR Dynamical Aspects. The ^{31}P DQ experiment displayed on Figure 8 gives the correct phosphorus site assignment by topology analysis without resorting to empirical correlations. P3 sites are dedoubled because of the water structure as rationalized previously. For all the cross-peaks of the P3 sites, an unexpected low intensity is observed. Close inspection of rows and column of the 2D experiment was necessary to detect all the expected intensities.

How come such low intensities are obtained only for the cross-peaks related to P3? One must have a mechanism that shortens the T_2^{DQ}, reducing then the observation of these lines. One cannot invoke a dipolar coupling to the hydrogen reservoir of the diamines, because if this would be so, no specificity would be expected for P3 compared with the other phosphorus sites. But fluctuations of water molecules around P3 sites are likely to play a crucial role. The structural model built leaves empty sites for water according to the global fractional occupancy factors. Molecules can actually occasionally jump in and out of these empty sites. But these jumps occur only between definite crystallographic sites. They cannot be fast, otherwise P3 chemical shifts would not be differentiated. They cannot be random either, for the same reason; P3 sites would then be distributed and would lead to one single broad P3 line. As a consequence, correlated jumps leaving the periodic pattern unchanged should occur and modulate the P—H dipolar pattern,
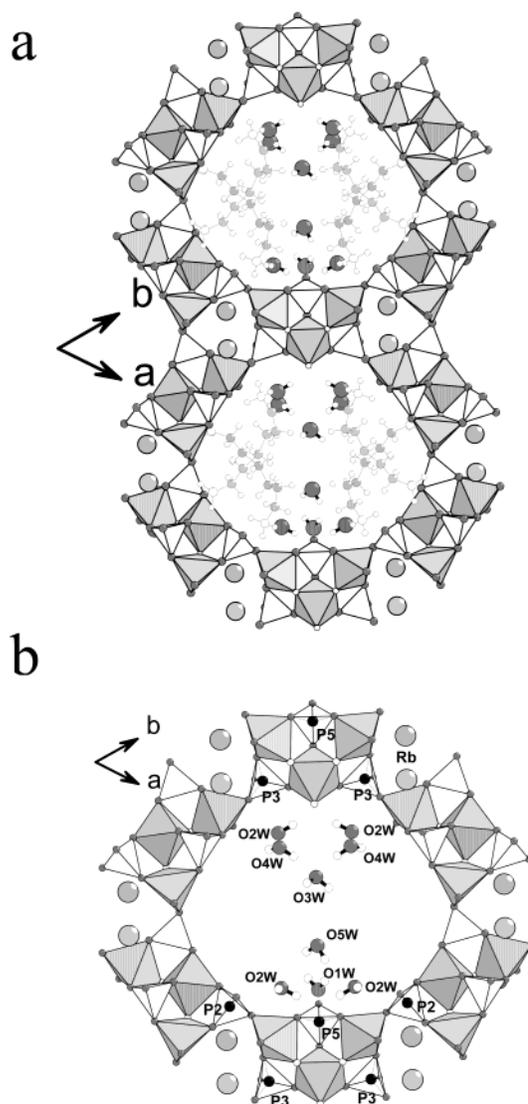

Figure 9. Water patterns in MIL-50 in the low symmetry description (space group $P1$). (a) View along c showing the water molecules (dark gray) confined between the hydrophobic part of the diamine and the "walls" of the inorganic framework; (b) details of the two water sublattices along c. Amines have been omitted for clarity.

creating a mechanism for shortening specifically P3 T_2^{DQ}. The modulation frequency cannot be higher than the phosphorus chemical shift frequency difference, that is, here about 1 ppm at 11.7 T, about 200 Hz for the jumping frequency, and 5 ms or longer for the residence period. Such a time is extremely similar to those found on silica surfaces for creeping water. The jumps of water keep however the overall periodicity invariant. The P3 sites exhibit hence a lower multiplicity than that in diffraction analysis.

Both XRD analysis and the partial charge scheme are based on a static model for a given geometry. Water molecules are however fluctuating, as indicated later in the DQ NMR experiment. These fluctuations are not taken into account in both static descriptions (XRD and charge calculations), and a more detailed model of positions and motions cannot be proposed yet. However, these fluctuations keep P3 sites split, indicating discrete jumps between inequivalent water sites in the water sublattice. They may contribute to some additional averaging of all phosphorus sites other than P3.

Structure Dynamics. Inclusion of Rb in the framework changes the assembling properties. Fewer templates are needed for charge compensation, and this frees room for some water in the pores. Water localizes close to P3 specifically, reorients, and hops or is moved by the network fluctuations, to diffuse to another available site. If the motion were fast (faster than the difference in frequency of both P3 phosphorus), then the averaged structure by diffraction and NMR would have been identical. If the motion is slow, then its maximum effect is sensed on P3, the site where the water is half localized. If the motion is frozen completely, one may expect that the symmetry of the whole network would be affected, not only P3 but also all other Pi at various degrees of sensitivity.

This is an example of incomplete differentiation between the two sublattices of the inorganic framework and the water network. Water might be considered to be just hosted in the inorganic framework or, oppositely, considered to be included as a part of the framework.

If the first description choice is made, then the symmetry of the crystal is just the symmetry of the inorganic framework (emphasized in a first analysis of XRD results). If the second choice is made, then the symmetry should be lowered in order to fit the water sublattice. Actually, one usually describes with the first choice and tolerates a lowering of one or several sites of multiplicities, as here with P3 sites because of the "contact" with the lower symmetry water sublattice. The water sublattice influences only P3 phosphorus site multiplicity, without having a measurable effect on the other phosphorus sites of the framework. Therefore, both the framework and the water sublattices can be more fully described by the structural model proposed previously.

Conclusion

A new open-framework structure has been obtained, by assembling hexameric units of Ga_3P_3 type, and it consists of large 18-ring channels encapsulating 1,6-diaminohexane species and water molecules. Additionally to these features, common to several already identified structures, rubidium atoms were incorporated in the framework and trapped within the small 6-ring channels. This is a configuration that has not been yet observed in comparable open-framework compounds. In the pores of this open framework, more room than usual is left, in which some water molecules are localized.

The mobile water molecules are inside the 18-ring cavities and move inside them, most probably along the c axis. Rubidium, in contrast, is localized in 6-ring channels along c. There is therefore no obvious reason why the water should meet rubidium. The latter stays therefore "dry". MIL-50 appears as a fascinating material, made of hexameric units, including "dry" rubidium atoms and hopping water within small ponds attached to the inorganic framework in the vicinity of the phosphate groups P3 and P5.

The water sublattice is formed of a periodic pattern of tiny ponds of lower symmetry than that of the framework. The interaction is weak enough to allow water to exchange within the available sites of one small pond. The hopping exchange modulates the DQ ^{31}P signals of P3, specifically, weakening the DQ intensities. Though detected by NMR, this symmetry lowering is not detected in diffraction.

MIL-50 is thus a very nice example demonstrating how different space groups may be invoked for a single structural model, depending on the measurement sensibility to the actual experimental parameters, here XRD and NMR. It shows also that hybrid situations where different symmetries can coexist within the same unit cell can very well be encountered, leading to partial symmetry lowering, that PACHA computations can easily model. Solid-state NMR appears well suited for pointing out the existence of such a superposition of space groups within the same unit cell. Actually, it is demonstrated in this example that only the full combination (diffraction, NMR and computational modeling) is able to handle in a way that may be brought down to *routine* analysis the fascinating complexity of microporous solid-state chemistry.